Available online at www.sciencedirect.com
ScienceDirect
Journal of Magnetism and Magnetic Materials 313 (2007) 98–106
Journal of magnetism and magnetic materials
www.elsevier.com/locate/jmmm

Magneto-optic imaging: Normal and parallel field components of in-plane magnetized samples

H. Ferrari[a,*], V. Bekeris[a], M. Thibeault[b], T.H. Johansen[c]

[a]*Laboratorio de Bajas Temperaturas, Departamento de Física, FCEyN, Universidad de Buenos Aires, CONICET, Argentina*
[b]*Departamento de Física, FCEyN, Universidad de Buenos Aires, Argentina*
[c]*Department of Physics, University of Oslo, Oslo, Norway*

Received 15 August 2006; received in revised form 27 October 2006
Available online 22 December 2006

Abstract

Magneto-optical (MO) imaging has become a powerful tool for determining magnetic properties of materials by detecting the stray magnetic fields. The technique consists in measuring the Faraday rotation, θ_F, in the light polarization plane when light travels through a transparent sensitive garnet (ferrite garnet film, FGF) placed in close contact to the sample. For in-plane magnetized samples, the MO image is not trivially related to the sample magnetization, and to contribute to this understanding we have imaged commercial audio tapes in which computer-generated functions were recorded. We present MO images of periodically in-plane magnetized tapes with square, sawtooth, triangular and sinusoidal waveforms, for which we analytically calculate the perpendicular and parallel stray magnetic field components generated by the tape. As a first approach we correlate the measured light intensity with the perpendicular magnetic field component at the FGF, and we show that it can be approximated to the gradient of the sample magnetization. A more detailed calculation, taking into account the effect of both field components in the Faraday rotation, is presented and satisfactorily compared with the obtained MO images. The presence of magnetic domains in the garnet is shown to be related to the change in sign of the parallel component of the stray magnetic field, which can be approximated to the second derivative of the sample magnetization.

Keywords: Magneto-optics; Indicator magnetic domain; In-plane; Out of plane magnetization

1. Introduction

Magneto-optical (MO) imaging provides a powerful tool for the direct observation of magnetic flux distributions in a wide variety of samples, ranging from magnetic to superconducting materials [1]. The visualization technique is based on the Faraday rotation of a polarized light beam illuminating an in-plane magnetized ferrite garnet film (FGF) placed directly on top of the sample surface. The light passes through the FGF and is reflected on a thin mirror layer deposited on its back face, and passes a second time through the garnet film, thus doubling the Faraday rotation angle, θ_F. In general, the rotation angle grows with the magnitude of the local magnetic field perpendicular to the FGF. By using a pair of polarizers in an optical microscope one can directly visualize and quantify the field distribution across the sample area. The samples magnetic properties are then modelled to reproduce the measured magnetic stray field.

The fast response of the FGF allows for a very high time resolution. Observations in the nanosecond time scale have been performed using a synchronized pulsed laser in a pump and probe technique [2]. The laser pulse is here split in two, with one part triggering a magnetic event, e.g., a flux avalanche in a superconductor, while the second part is optically delayed and used to take an MO snapshot of the moving flux [3].

Recently, also very high spatial resolution was achieved by detecting single superconducting vortices [4]. In these experiments, a very thin FGF is mounted within a minimum distance above the superconductor surface so that the exponential decay of the magnetic field modulation away from the surface remains small, thus allowing for

*Corresponding author. Tel.: +54 1 145763300; fax: +54 1 145763357.
E-mail address: hferrari@df.uba.ar (H. Ferrari).

0304-8853/$ - see front matter © 2007 Elsevier B.V. All rights reserved.
doi:10.1016/j.jmmm.2006.12.013

detection of one flux quantum provided the inter-vortex distance is not too small.

These achievements have been made in cases where the sample magnetization, $\vec{M}$, had a strong component perpendicular to the sensitive garnet. Even in these cases the correlation between the light intensity and the sample magnetization is complex because only the stray field is observed and the field at the place of the FGF may have a direction and magnitude very different from that of the sample's $\vec{M}$. An example is a thin film superconductor placed in a perpendicular applied magnetic field, where the magnetization is perpendicular to the superconductor film, whereas the outside field is largely parallel to the surface. An additional complication is that the garnet itself responds not only to a perpendicular field, but also to the stray field component parallel to the FGF [5,6].

Regarding in-plane magnetized samples, these have been also investigated with this technique. Bennet and collaborators [7], in their seminal work, studied the ferrimagnetic indicator film technique to observe magnetic domains in multilayer films with in-plane magnetization. A qualitative description was presented, particularly for holes in the multilayer film [7], which generate stray field with a component perpendicular to the indicator.

Periodically in-plane magnetized samples can be provided by the well-known tape recording technique [8]. These are excellent samples for addressing quantitative MO imaging experiments. In the past we have modelled square and sawtooth magnetized tapes by an array of coaxial circular coils where the current in each coil reproduced the recorded functions [9] to describe the observed light intensities in images. However, a formal correlation between image contrast and regions where the sample magnetization had strong variations was missing, and parallel field components had to be taken into account [5,6] to better understand light distribution. Therefore, in the present work, we examine square, sawtooth, triangular and sinusoidal waveforms by MO imaging and we provide an analytic calculation of the magnetic field generated by the tapes at a plane in close proximity to the sample. These calculations straightforwardly show that the perpendicular magnetic field component, at a plane in close proximity to the sample, is approximately equal to the magnetization gradient of the sample. Furthermore, we discuss in which cases the approximation is valid. Additionally, we prove mathematically that the parallel field component cannot be approximated to the second derivative of $\vec{M}$, but that both have their maxima, minima and zeros at the same positions. In consequence, inspection of the MO image of in-plane magnetized samples, readily allows the determination of the space variation of the sample magnetization, as well as the locations where the parallel field component changes sign.

The paper is organized as follows. Section 2 describes the experimental details and the obtained MOI results. In Section 3 analytical calculations of the stray magnetic field components are presented, followed by Section 4 with a discussion of experimental and theoretical results. Finally, the conclusions are drawn in Section 5.

2. Experimental results

The physics of tape recording is well understood [10]. The signal to be recorded is conditioned to activate a writing head through its coil-wound core, generating a signal on the tape that is a direct spatial reproduction of the original temporal signal. Bi-polar square, sawtooth, triangular and sinusoidal wave functions were computer generated and recorded on commercial audio tapes.

We used here 100 Hz audiosignals for which tapes with linear velocity $v = \frac{15}{8}$ in per second during recording, produced samples magnetized with a spatial periodicity $l = 0.475$ mm. Fig. 1(a) shows schematically the recorded magnetization profiles. To determine the maximum magnetization m_0 per unit area, a DC signal (i.e. $l = \infty$), with an amplitude equal to the peak amplitude, was recorded for some seconds and the recorded tape magnetic moment was measured with a Vibrating Sample Magnetometer at room temperature, resulting $m_0 = 0.164$ A.

The FGF we have used in the present work is a bi-doped garnet film, $Lu_{3-x}Bi_xFe_{5-y}Ga_yO_{12}$ with $x \sim 0.5$ and $y \sim 0.7$ with in-plane magnetization [5]. The indicator film was deposited to a thickness of 4.5 μm by liquid-phase epitaxial growth on the (1 0 0)-oriented gadolinium gallium garnet substrate.

A thin (~120 nm) Au layer was evaporated onto the film in order to reflect the incident light and thus to provide a double Faraday rotation of the light beam. To image each sample, the pair polarizer–analyzer was set slightly out of crossing so that perpendicular fields of opposite polarity were distinguished in the MO image, i.e. a medium gray color is representing zero field. This angle was fixed to $\theta_0 = 4^\circ \pm 10\%$ for all samples. The flexible samples were carefully placed under the indicator film, pressing both together so that the air gap between the sample and the FGF indicator was minimized. In calculations, the finite distance between the sample surface and the FGF was taken into account, i.e. the magnetic field is calculated at a distance $\frac{1}{100}\, l$, where l is modulation period.

A standard Olympus $B \times 60M$ microscope was used with 10× magnification, and a Roper Scientific CoolSnap cf camera recorded the images, which were transferred to a computer for processing.

Fig. 1(b) shows MO images obtained for magnetized tapes having the four different in-plane magnetization waveforms shown in the corresponding adjacent schematic. Each image includes 1.5 spatial periods.

In what follows we will refer to the coordinate system shown in the inset of Fig. 2.

The observation of images leads us to the following approximate description. The bright and dark lines in the top image of Fig. 1(b) correspond to positive and negative magnetic field components H_z that arise from the abrupt decrease (from m_0 to $-m_0$) and increase (from $-m_0$ to m_0)

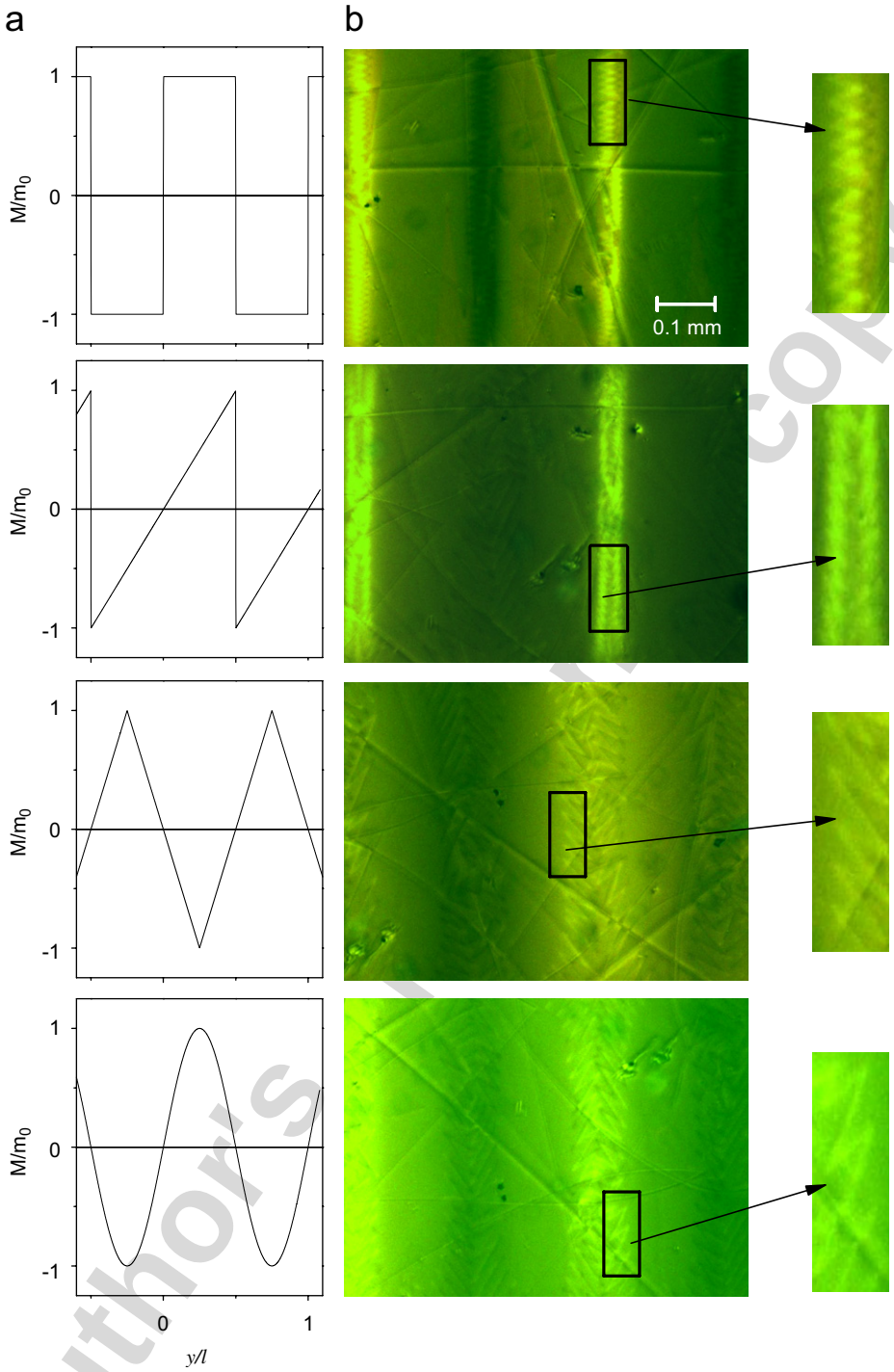

Fig. 1. (a) Sample magnetization in units of m_0 for the square, sawtooth, triangular and sinusoidal magnetization wave forms. (b) MO images of four different tapes magnetized with a square, sawtooth, triangular and sinusoidal audio waveform of 100 Hz, in panels from top to bottom. The bright areas represent strong positive magnetic field, and the darker areas strong negative magnetic field perpendicular to the tape. The distance between two consecutive bright lines is ~0.5 mm. See text. To the right enlarged areas show zigzag domains in the garnet, appearing where the parallel field component changes sign.

in the in-plane component of magnetization, $M_y = \mathscr{M}(y)$, for the square waveform plotted in Fig. 1(a). In the second row, the bright lines indicating $H_z > 0$, correspond to the abrupt decrease in $\mathscr{M}(y)$ (from m_0 to $-m_0$) for the sawtooth waveform, and the constant intensity observed between bright lines is related to the constant slope of the sawtooth signal. In the third row, the intensity varies following the corresponding triangular waveform. A similar result is observed for the sinusoidal waveform, shown in the bottom row. The first observation is that light intensity seems to scale with the derivative of the in-plane magnetization, $\mathrm{d}\mathscr{M}(y)/\mathrm{d}y$. In the next section we will show

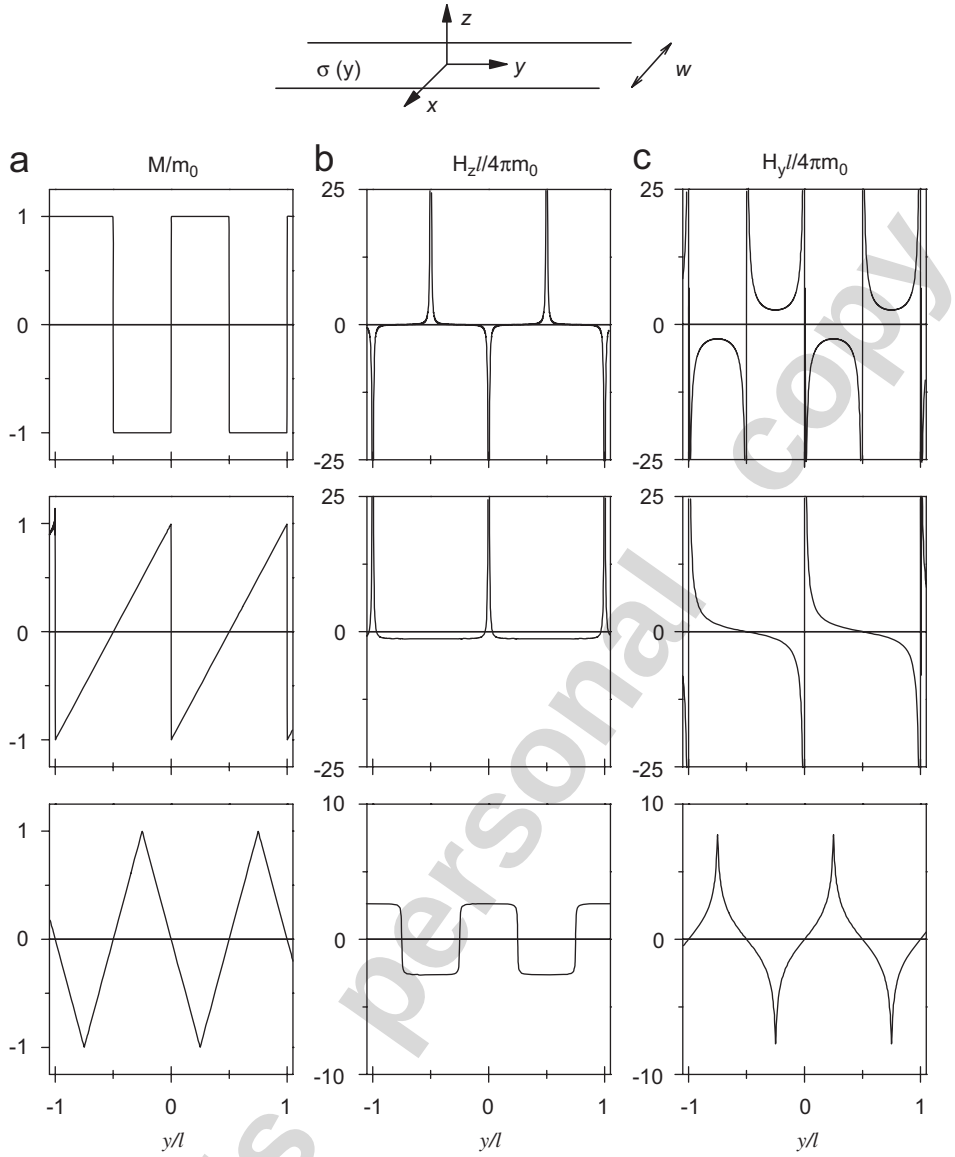

Fig. 2. Inset: strip of width w with in-plane magnetization dependent on coordinate y. (a) Sample magnetization in units of m_0 (same as in Fig. 1(a)) for the square, sawtooth and triangular magnetization wave forms of wavelength l. (b) Calculated perpendicular magnetic field component, H_z, in units of $4\pi m_0 l^{-1}$ for the square, sawtooth and triangular magnetization waveforms of wavelength l, from top to bottom panels. (c) Calculated parallel magnetic field component, H_y, in units of $4\pi m_0 l^{-1}$ for the square, sawtooth and triangular magnetization waveforms of wavelength l, from top to bottom panels.

that this result is a good approximation, if θ_F is correlated to the perpendicular field component and the FGF is near the sample surface.

A close inspection of the MO images in Fig. 1(b) shows that in the dark and bright regions zigzag domain walls are present [11]. These domains are formed in the garnet itself, each having the garnet in plane magnetization component pointing oppositely. We will show that the domain walls appear at regions where the parallel field component at the garnet changes sign, in the same way as was already shown for out-of-plane magnetized samples [11].

In the following section we calculate the magnetic field components for the different magnetized tapes and we show their relation to the first and second derivatives, $\mathrm{d}\mathscr{M}(y)/\mathrm{d}y$ and $\mathrm{d}^2\mathscr{M}(y)/\mathrm{d}y^2$ of the sample magnetization.

3. Modelling

We present our calculations for the magnetic field $\vec{H}$ generated by a magnetized tape with periodic in-plane magnetization. The aim is to calculate the normal and parallel field components created by periodically magnetized strips, as well as to find the relation between these field components and the magnetization first and second derivatives. In the next section, we will use these results to calculate the light intensity of MO images and we will also relate image contrast with sample magnetization.

The tape is modelled by an infinite strip of width $-w/2 \leqslant x \leqslant w/2$ and thickness $-s/2 \leqslant z \leqslant s/2$, see the inset of Fig. 2, where the x independent in-plane magnetization is $\vec{M} = M_y(y)\hat{\mathbf{y}}$ [12]. For the purpose of this work we will

take the limit $s = 0$. We recall that the Maxwell equation for a source with magnetization and without free current is:

$$\vec{\nabla} \times \vec{H} = 0, \tag{1}$$

$$\vec{\nabla} \cdot \vec{H} = -4\pi \vec{\nabla} \cdot \vec{M}. \tag{2}$$

It is convenient to think the divergence on the right-hand side of Eq. (2) as a volumetric (magnetic) charge density $\rho_M \equiv -\vec{\nabla} \cdot \vec{M}$. We will consider that the magnetization is confined to the xy plane, with width w in the x direction and of infinite length in the y direction, so that

$$\vec{M} = \mathscr{M}(y)[\Theta(x + w/2) - \Theta(x - w/2)]\delta(z)\hat{y}, \tag{3}$$

where $\delta(z)$ is Dirac delta and $\Theta(x)$ is the boxcar function. Note that $\mathscr{M}$ has units of magnetic moment per unit area.

We also assume that the magnetization is periodic with period l and consequently can be written as a Fourier expansion

$$\mathscr{M}(y) = \sum_{n=0}^{\infty} \left\{ b_n \cos\left(\frac{2\pi n}{l} y\right) + a_n \sin\left(\frac{2\pi n}{l} y\right) \right\}. \tag{4}$$

The volumetric charge density reduces to $\rho_M = \sigma(y)\delta(z)$. Introducing the magnetic potential ϕ_M such that $\vec{H} = -\vec{\nabla}\phi_M$ leads to the following differential equation:

$$\nabla^2 \phi_M = -4\pi\sigma\delta(z), \tag{5}$$

where

$$\sigma = -\frac{\partial \mathscr{M}(y)}{\partial y}[\Theta(x + w/2) - \Theta(x - w/2)]. \tag{6}$$

The solution is straightforwardly obtained [13] to be:

$$\phi(x, y, z) = -\frac{4}{l} \sum_{n=0}^{\infty} \int \mathrm{d}k_x \frac{\mathrm{e}^{-k|z|}}{k k_x} \sin\left(\frac{k_x w}{2}\right) \cos(k_x x) \times \left(I_C(n) \cos\left(\frac{2\pi n}{l} y\right) + I_S(n) \sin\left(\frac{2\pi n}{l} y\right) \right), \tag{7}$$

$$I_C(n) = \int_{-l/2}^{l/2} \frac{\partial \mathscr{M}(y)}{\partial y} \cos\left(\frac{2\pi n}{l} y\right) \mathrm{d}y, \tag{8}$$

$$I_S(n) = \int_{-l/2}^{l/2} \frac{\partial \mathscr{M}(y)}{\partial y} \sin\left(\frac{2\pi n}{l} y\right) \mathrm{d}y, \tag{9}$$

$$k = \sqrt{\left(\frac{2\pi n}{l}\right)^2 + k_x^2}. \tag{10}$$

It is convenient to write explicitly the potential using the Fourier coefficients of the magnetization. The magnetic charge density is given by Eq. (6) and to simplify, we do not write explicitly the Heaviside functions, so that

$$\sigma = -\frac{\partial \mathscr{M}(y)}{\partial y} = \sum_{n=0}^{\infty} \left\{ -\frac{2\pi n}{l} a_n \cos\left(\frac{2\pi n}{l} y\right) + \frac{2\pi n}{l} b_n \sin\left(\frac{2\pi n}{l} y\right) \right\}. \tag{11}$$

Therefore, $I_C(n) = -\pi n a_n$ and $I_S(n) = \pi n b_n$. We can thus write the magnetic potential as:

$$\phi(x, y, z) = -\frac{4\pi}{l} \sum_{n=0}^{\infty} \int \mathrm{d}k_x \frac{\mathrm{e}^{-k|z|}}{k k_x} \sin\left(\frac{k_x w}{2}\right) \cos(k_x x) \times \left\{ n a_n \cos\left(\frac{2\pi n}{l} y\right) - n b_n \sin\left(\frac{2\pi n}{l} y\right) \right\}. \tag{12}$$

The case of interest here is when $|z| = \varepsilon \ll w$. Up to now the only approximation was to consider the magnetic tape as bi-dimensional. Under this restriction, the analytical solution is exact but not very intuitive. However, upon the assumption of very small distance from the xy plane, we can obtain an approximate result that fits very satisfactorily the observed experimental results as will be shown below.

Let us make the change of variable $k_x \to u = \varepsilon k_x$. We obtain

$$\phi = -\frac{4\pi}{l} \sum_{n=0}^{\infty} \int \mathrm{d}u \frac{\mathrm{e}^{-k|\varepsilon|}}{ku} \sin\left(\frac{uw}{2}\frac{1}{\varepsilon}\right) \cos\left(\frac{ux}{\varepsilon}\right) \times \left\{ n a_n \cos\left(\frac{2\pi n}{l} y\right) - n b_n \sin\left(\frac{2\pi n}{l} y\right) \right\}.$$

Now $\sin((uw/2)1/\varepsilon)\cos(ux/\varepsilon) = \frac{1}{2}\sin[u/\varepsilon(x + w/2)] + \frac{1}{2}\sin[u/\varepsilon(x - w/2)]$.

Note that for $\eta = \pm 1$, we can evaluate the limit:

$$\lim_{\varepsilon \to 0} \frac{\sin[u(x + \eta(w/2))1/\varepsilon]}{u} = \lim_{\varepsilon \to 0} \frac{\sin[u(x + \eta(w/2))1/\varepsilon]}{u(x + \eta w/2)} \times (x + \eta w/2) = (x + \eta w/2)\delta(u(x + \eta w/2)) = \delta(u).$$

The previous reasoning is valid if $x \neq -\eta w/2$. The idea is then to approximate

$$\frac{\sin[u/\varepsilon(x + \eta(w/2))]}{u} \to \delta(u).$$

Therefore,

$$\sin\left(\frac{uw}{2}\frac{1}{\varepsilon}\right) \cos\left(\frac{ux}{\varepsilon}\right) \to \delta(u)$$

is valid if x is not too near the border of the tape. We can now proceed with the integration over u to obtain

$$\phi = -\frac{4\pi}{l} \sum_{n=0}^{\infty} \frac{\mathrm{e}^{-2\pi n|\varepsilon|/l}}{(2\pi n/l)} \times \left\{ n a_n \cos\left(\frac{2\pi n}{l} y\right) - n b_n \sin\left(\frac{2\pi n}{l} y\right) \right\}.$$

The physical quantities of interest are the z and y components of the magnetic field $\vec{H}$:

$$H_z = -\frac{4\pi}{l} \sum_{n=0}^{\infty} \mathrm{sg}(\varepsilon)\mathrm{e}^{-2\pi n|\varepsilon|/l} \times \left\{ n a_n \cos\left(\frac{2\pi n}{l} y\right) - n b_n \sin\left(\frac{2\pi n}{l} y\right) \right\}, \tag{13}$$

$$H_y = -\frac{4\pi}{l}\sum_{n=0}^{\infty} e^{-2\pi n|\varepsilon|/l} \times\left\{na_n \sin\left(\frac{2\pi n}{l}y\right) + nb_n \cos\left(\frac{2\pi n}{l}y\right)\right\}. \quad (14)$$

Note that for $|z| = \varepsilon \ll l$, and if high frequencies are not relevant, the exponential factor $e^{-2\pi n|\varepsilon|/l} \approx 1$ in Eq. (13).

In this case the perpendicular component of the magnetic field can be approximated to the gradient of the magnetization, Eq. (11). On the other hand, the y component of the magnetic field (Eq. (14)) can be approximated to the second derivative of $\mathcal{M}(y)$ although the relation is more restricted. Consider the case where the magnetization has a definite parity, say odd. Then, the second derivative of $\mathcal{M}(y)$ will also be odd, as will be the case for H_y. Then, $\partial^2\mathcal{M}(y)/\partial y^2$ and H_y will have their minimum, maximum and zeros at the same place.

To validate our approximation, we have to confront its prediction with the experimental results. Let us then analyze some examples of magnetization.

The first example is a square signal:

$$\mathcal{M}(y) = \begin{cases} m_0, & 0 < y < l/2, \\ -m_0, & -l/2 < y < 0, \end{cases}$$

which can be represented by the following Fourier series:

$$\mathcal{M}(y) = \sum_{k=0}^{\infty} \frac{4m_0}{\pi(2k+1)} \sin\left(\frac{2\pi(2k+1)}{l}y\right).$$

The square magnetization waveform is plotted in units of m_0 in Fig. 2(a), top row. In panel (b) top row, the z component of the magnetic field, $H_z(y/l)$, slightly above the tape using our approximation of Eq. (13) is shown in units of $4\pi m_0 l^{-1}$. Additionally, the y component of the magnetic field, $H_y(y/l)$, (in the same units), slightly above the tape as calculated in Eq. (14) is plotted in panel (c) top row.

The second example is a sawtooth signal, expressed as:

$$\mathcal{M}(y) = \frac{2m_0}{l}y - m_0$$

with the corresponding Fourier expansion:

$$\mathcal{M}(y) = -\sum_{n=1}^{\infty} \frac{2m_0}{\pi n} \sin\left(\frac{2\pi n}{l}y\right).$$

Graphically, we have for $\mathcal{M}(y/l)$ the plot in Fig. 2(a) second row, and the z and y components of the magnetic field are shown in panels (b) and (c) second row, respectively.

As third example, we present a triangular signal, plotted in Fig. 2(a) third row:

$$\mathcal{M}(y) = \begin{cases} 2m_0 + \frac{4m_0}{l}y, & -\frac{l}{2} \leqslant y \leqslant -\frac{l}{4}, \\ -\frac{4m_0}{l}y, & -\frac{l}{4} \leqslant y \leqslant \frac{l}{4}, \\ -2m_0 + \frac{4m_0}{l}y, & \frac{l}{4} \leqslant y \leqslant \frac{l}{2}. \end{cases}$$

The Fourier series is

$$\mathcal{M}(y) = -\sum_{k=0}^{\infty} \frac{8w(-1)^k}{\pi^2(2k+1)^2} \sin\left(\frac{2\pi(2k+1)}{l}y\right).$$

Our result for the z component of the magnetic field is plotted in panel (b) third row. Finally, the y component of the magnetic field is shown in Fig. 2(c) third row. Note that in this case, both components are plotted in a more sensitive scale. We do not plot results for the sinusoidal waveform, because they are straightforward.

4. Discussion

Calculations have shown that for the four different magnetization waveforms, the perpendicular component of the stray field near the sample surface, H_z, is approximately proportional to $-d\mathcal{M}/dy$ and that the parallel component H_y has its minimum, maximum and zeros at the same place as $d^2\mathcal{M}/dy^2$. If one assumes that Faraday rotation is determined by the perpendicular field component at the garnet position, then the MO image provides information of the derivative of the strip magnetization, as was deduced empirically by observing the images shown in Fig. 1.

However, in our calculations we have shown that for the magnetic field components near the sample, only the higher Fourier harmonics are attenuated by the exponential factor (see Eqs. (13) and (14)), so that the quality of the approximation depends on the relevance of the high frequency terms in the gradient of the magnetization: if these are not relevant then the approximation is good (as in the case of the square or sawtooth waveforms). This explains why for the triangular waveform, the field components seem not to be so well described by the first and second derivatives of the magnetization.

Before we proceed to compare experimental results with calculations, let us present some remarks regarding the role of both the perpendicular and parallel field components in MO imaging.

Linearly polarized light propagating through the FGF will experience a rotation of its polarization vector if a magnetic field is present [4,5]. The Faraday effect relates to the fact that the FGF is a ferrimagnet having a spontaneous magnetization, M_s, with the easy axis lying in the film plane. An external magnetic field $\vec{H}$ at an angle α will force the magnetization vector out of the plane, see Fig. 3(a), while the magnetization is essentially constant in magnitude. The equilibrium tilt angle η of M_s represents

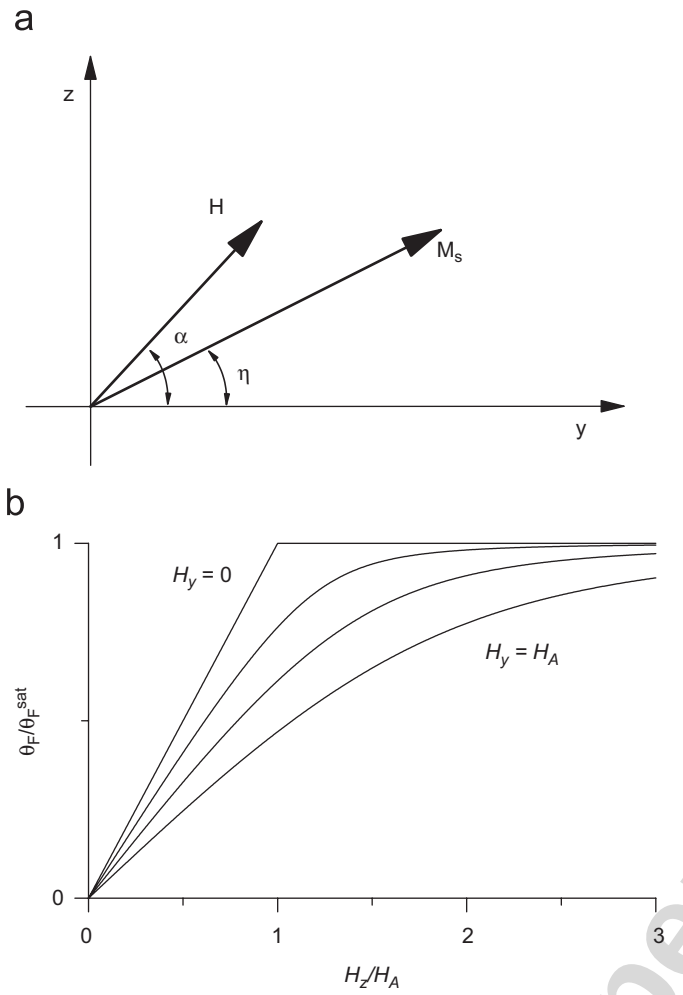

Fig. 3. (a) The spontaneous magnetization, M_s, of the ferrite garnet film (FGF) has an easy axis lying in the film plane. An external magnetic field $\vec{H}$ at an angle α forces M_s out of the plane. The equilibrium tilt angle η represents the balance between the shape anisotropy and the tendency to align with the external field, and determines the Faraday rotation, θ_F, of the linearly polarized light (see text). (b) If the field has a component H_y parallel to the FGF, θ_F is slightly reduced. Polarization rotation θ_F as a function of H_z for different parallel field components, $H_y = 0$, $H_A/5$, $H_A/2$ and H_A.

the balance between the shape anisotropy and the tendency to align with the external field. In the simplest form this can be expressed as a minimum of

$$K_1 \sin^2(\eta) - HM_s \cos(\alpha - \eta), \tag{15}$$

where K_1 is the anisotropy energy volume density. The anisotropy term in Eq. (15) has a different form than the one used in Ref. [5], which we believe now is incorrect.

Minimizing Eq. (15) with respect to η gives

$$\frac{H_z}{\sin(\eta)} - \frac{H_y}{\cos(\eta)} = \frac{2K_1}{M_s} \equiv H_A. \tag{16}$$

The Faraday rotation, θ_F, is proportional to the component of M_s along the light beam direction, so that

$$\theta_F = \theta_F^{sat} \sin(\eta), \tag{17}$$

where θ_F^{sat} is the maximum rotation angle. When only a perpendicular field is present, i.e., $H_y = 0$, it follows from Eq. (16) that for $H_z \leqslant H_A$,

$$\theta_F = \theta_F^{sat} \frac{H_z}{H_A}, \tag{18}$$

giving a simple linear relation between the field and the Faraday rotation shown in Fig. 3(b). When the field exceeds H_A the Faraday rotation remains constant. Since θ_F^{sat} is proportional to the film thickness, t, the FGF characteristics can also be expressed in the more familiar form,

$$\theta_F = VH_z t, \tag{19}$$

where V is the Verdet constant.

If the field also has a parallel component H_y, the expression for θ_F is modified according to Eq. (16), which gives a slight reduction in the Faraday effect. Fig. 3(b) shows $\theta_F(H_z)$ for different parallel field components, $H_y = 0$, $H_A/5$, $H_A/2$ and H_A. The fact that the effect is small justifies our first approach in which only the perpendicular field component determines the polarization rotation and gives a linear relation between θ_F and H_z (see Eq. (18)). For the films used in the present studies, calibration experiments show that $H_A \approx 6.4 \times 10^4\,\mathrm{A/m}$ and $\theta_F^{sat} \approx 5^\circ$, giving a sensitivity of $V \approx 8^\circ/\mu\mathrm{m\,A/m}$ [4].

After the light is rotated by the FGF and reflected by the mirror layer, the beam re-enters the objective lens. In the microscope a second polarizer (analyzer) filters the light according to Malus' law. With the analyzer set at $90^\circ + \theta_0$ relative to the original polarization, the intensity distribution arriving at the camera becomes

$$\frac{I(y)}{I_0} = \sin^2(\theta_F(y) + \theta_0) + E \approx (\theta_F(y) + \theta_0)^2 + E. \tag{20}$$

Here I_0 is the intensity before the analyzer and E is the effective extinction ratio of the optical system, which is negligible, $E = (1-3)10^{-4}$ and θ_0 is the analyzer–polarizer uncrossing. Combining this with the characteristics of the FGF it follows that at magnetic fields below H_A the light intensity versus magnetic field is a parabolic function.

It then becomes clear that in our first simplified approach we have made several approximations: we related the observed light intensity only to the perpendicular field component and we approximated the perpendicular field component to the derivative of the magnetization. Moreover, the light intensity is quadratic in H_z, but this last dependence is not detected by naked eye observation, and describes qualitatively the observed intensity.

Fig. 4(a) shows the measured light intensity $I(y)$ in arbitrary units, after averaging it along the width of the tape (x direction). The four rows, from top to bottom, represent results for the square, sawtooth, triangular and sinusoidal waveforms. To the right, in panels (b), we have plotted the calculated $H_z(y, \varepsilon)$ in units of $4\pi m_0 l^{-1}$. H_z was shown to be approximately proportional to $-\mathrm{d}M/\mathrm{d}y$ (see Section 2). We find that $I(y)$ is qualitatively described by

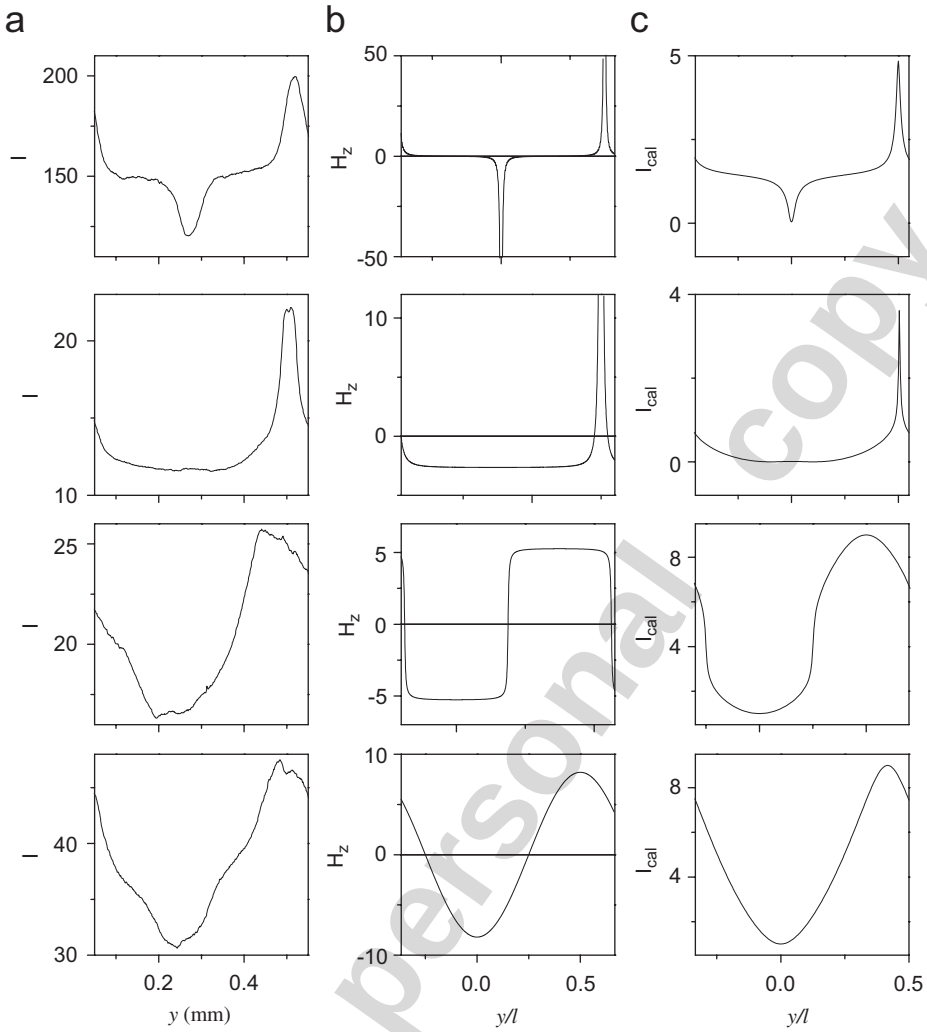

Fig. 4. (a) The four panels from top to bottom show the measured light intensity I in arbitrary units as a function of y, averaged along x (see inset in Fig. 2), for the square, sawtooth, triangular and sinusoidal magnetization waveforms. (b) The four panels from top to bottom show the calculated $H_z(y,\varepsilon)$ (also shown in Fig. 2(b), except for the sinusoidal waveform) for the square, sawtooth, triangular and sinusoidal magnetization waveforms. (c) The four panels show the calculated light intensity, including the effect of the parallel field component and the initial polarizer–analyzer crossing, neglecting the extinction ratio E (see text).

the magnetization gradient, and therefore the image can be used to estimate the variation of M with position.

However, the correct calculation of light intensity is plotted in Fig. 4(c) and it clearly adjusts better to the experimental results. Particularly for the square waveform, top panels, the different dip and peak heights observed in (a) are reproduced in (c), because the analyzer and polarizer were not completely crossed and an additional phase was added to θ_F in Eq. (20) (see Section 2). For the sawtooth waveform, second row, the curvature of $I(y)$ is reproduced satisfactorily, and the measured intensity for the triangular waveform (third row from the top) is well described by the calculated intensity plotted in (c). The description is also more satisfactory for the sinusoidal waveform in the bottom row. Observe that the valley in the light intensity is wider than the crest, feature that is reproduced by the calculated I but not by $H_z(y)$.

The smeared features in the measured light intensity have been reproduced by including the parallel field component contribution. However we must point out that calculated light intensity is strongly dependent on the distance of the FGF to the sample surface, and for larger distances the smearing of light intensity may not be dominated by the parallel field component contribution, but only by the perpendicular field component dependence with the distance to the sample surface.

The observed profile asymmetry on symmetric structures is due to the asymmetry of the right and left Faraday rotation relatively to the polarizers (the pair polarizer–analyzer was set slightly out of crossing so that perpendicular fields of opposite polarity are distinguished in the MO image). It can be corrected by subtraction of two images obtained with opposite polarizers uncrossing as shown in Ref [14], but was not done in the present work.

A structure in some of the peaks in Figs. 4(a) can be observed even after having averaged the signal along the tape width, and this structure is related to the presence of induced magnetic domains in the garnet (see images in Fig. 1(b)). Note that these domains coincide with the change in sign of the parallel component of the magnetic field, H_y, plotted in Fig. 2(c) [11]. This description is valid for all studied waveforms.

The zigzag domains in the indicator have been used in the past to experimentally plot the profile of the parallel field above a superconductor in the absence of perpendicular component [15] by applying an external parallel field, and observing the displacement of the zigzag domain walls. In addition the presence of domain walls could be used to detect sample misalignments.

5. Conclusions

Magneto-optical imaging of in-plane magnetized samples has been addressed. For this purpose, audio tapes were magnetized with square, sawtooth, triangular and sinusoidal audio-waveforms. The stray magnetic field generated by the tapes was calculated analytically, modelling the magnetic tapes as infinite strips, with periodic in-plane magnetized waveforms. Calculations were made near the sample surface to describe the field where the MO indicator was placed. MO images were compared with theoretical results, showing that the light intensity in the image follows qualitatively the calculated perpendicular field component. We have additionally found that the perpendicular magnetic field component can be approximated to the gradient of the in-plane magnetization, while the parallel field component approximates to the magnetization second derivative. The quality of these approximations reduces as the relevance of the higher harmonics in the Fourier transform of the magnetization waveform increases.

To obtain a more precise description, light intensity was calculated following the known equations for Faraday light rotation, where both the perpendicular and parallel field components contribute, and Malus law was applied. Experimental results are well reproduced by these calculations, particularly the smeared features that can be accounted for the contribution of the parallel field component and the distance of the garnet to the sample surface. The asymmetry observed in the light intensity is related to the asymmetric positioning of the pair polarizer–analyzer to distinguish perpendicular fields of opposite polarities.

The magnetic domains in the FGF are related to the parallel field component, and we have shown that the magnetic domains are spontaneously created in the garnet where the calculated parallel field component changes sign. We believe that this "artifact" could be used to detect sample misalignments, or the presence of external magnetic field components, in cases where domains are observed displaced from positions where symmetry arguments lead to the prediction of the change in sign of the parallel field component.

Acknowledgments

This work was partially supported by UBACyT EX200, CONICET PIP 5609/06 and Fundación Sauberán.

References

[1] M.R. Koblischka, R.J. Wijngaarden, Supercond. Sci. Technol. 8 (1995) 199;
Ch. Jooss, J. Albrecht, H. Kuhn, S. Leonhardt, H. Kronmüller, Rep. Prog. Phys. 65 (2002) 651.
[2] U. Bolz, D. Schmidt, B. Biehler, B.-U. Runge, R.G. Mints, K. Numssen, H. Kinder, P. Leiderer, Physica C 388–389 (2003) 715.
[3] P. Brüll, D. Kirchgassner, P. Leiderer, Physica C 182 (1991) 339.
[4] P.E. Goa, H. Hauglin, A.A.F. Olsen, M. Baziljevich, T.H. Johansen, Rev. Sci. Instrum. 74 (2003) 141.
[5] T.H. Johansen, M. Baziljevich, H. Bratsberg, Y. Galperin, P.E. Lindelof, Y. Shen, P. Vase, Phys. Rev. B 54 (1996) 16264.
[6] P. Paturi, Rev. Sci. Instrum. 76 (2005) 093908.
[7] L.H. Bennett, R.D. McMichael, L.J. Swartzendruber, S. Hua, D.S. Lashmore, A.J. Shapiro, V.S. Gornakov, L.M. Dedukh, V.I. Nikitenko, Appl. Phys. Lett. 66 (1995) 888.
[8] See for example: D. Mee, E. Daniel, Magnetic Recording Handbook, McGraw-Hill, New York, 1990.;
D. Wei, H.N. Bertram, F. Jeffers, IEEE Trans. Magn. 30 (1994) 2739.
[9] H. Ferrari, V. Bekeris, T.H. Johansen, Physica B 554 (2004) 365.
[10] See for example: R.C. O' Handley, Modern Magnetic Materials, Principles and Applications, Wiley, New York, 2000.
[11] V.K. Vlasko-Vlasov, L.A. Dorosinskii, M.V. Indenbom, V.I. Nikitenko, A.A. Polyanskii, R. Prozorov, Supercond. Phys. Chem. Technol. 6 (1993) 555.
[12] We omit coordinate x because there is no x dependence.
[13] J.D. Jackson, Classical Electrodynamics, Wiley, New York, 1966.
[14] R.J. Wijngaarden, K. Heeck, M. Welling, R. Limburg, M. Pannetier, K. van Zetten, V.L.G. Roorda, A.R. Voorwinden, Rev. Sci. Instrum. 72 (2001) 2661.
[15] M.V. Indenbom, H. Kronmüller, T.W. Li, P.H. Kes, A.A. Menovsky, Physica C 222 (1994) 203.